

Nodal Quasiparticle Meltdown in Ultra-High Resolution Pump-Probe Angle-Resolved Photoemission

J. Graf,^{1,*} C. Jozwiak,^{2,1,*} C.L. Smallwood,³ H. Eisaki,⁴ R. A. Kaindl,¹ D.-H. Lee,^{3,1} and A. Lanzara^{3,1,†}

¹*Materials Sciences Division, Lawrence Berkeley National Laboratory, Berkeley, CA 94720, USA*

²*Advanced Light Source, Lawrence Berkeley National Laboratory, Berkeley, CA 94720, USA*

³*Department of Physics, University of California, Berkeley, CA 94720, USA*

⁴*Superconducting Electronics Group, Electronics and Photonics Research Institute, National Institute of Advanced Industrial Science and Technology (AIST), 1-1-1 Central 2, Umezono, Tsukuba, Ibaraki 305-8568, Japan*

High- T_c cuprate superconductors are characterized by a strong momentum-dependent anisotropy between the low energy excitations along the Brillouin zone diagonal (nodal direction) and those along the Brillouin zone face (antinodal direction). Most obvious is the d -wave superconducting gap, with the largest magnitude found in the antinodal direction and no gap in the nodal direction. Additionally, while antinodal quasiparticle excitations appear only below T_c , superconductivity is thought to be indifferent to nodal excitations as they are regarded robust and insensitive to T_c . Here we reveal an unexpected tie between nodal quasiparticles and superconductivity using high resolution time- and angle-resolved photoemission on optimally doped $\text{Bi}_2\text{Sr}_2\text{CaCu}_2\text{O}_{8+\delta}$. We observe a suppression of the nodal quasiparticle spectral weight following pump laser excitation and measure its recovery dynamics. This suppression is dramatically enhanced in the superconducting state. These results reduce the nodal-antinodal dichotomy and challenge the conventional view of nodal excitation neutrality in superconductivity.

The electronic structures of high- T_c cuprates are strongly momentum-dependent. This is one reason why the momentum-resolved technique of angle-resolved photoemission spectroscopy (ARPES) has been a central tool in the field of high-temperature superconductivity.¹ For example, coherent low energy excitations with momenta near the Brillouin zone face, or antinodal quasiparticles (QPs), are only observed below T_c and have been linked to superfluid density.^{2,3} They have therefore been the primary focus of ARPES studies. In contrast, nodal QPs, with momenta along the Brillouin zone diagonal, have received less attention and are usually regarded as largely immune to the superconducting transition because they seem insensitive to perturbations such as disorder,⁴⁻⁶ doping,⁶⁻⁸ isotope exchange,⁹ charge ordering,^{6,10,11} and temperature.¹²⁻¹⁵ Clearly, finding any strong dependencies of the nodal QPs will alter the conventional view and enrich our understanding of high temperature superconductivity.

Time resolution through pump-and-probe techniques adds a new dimension to ARPES by directly measuring how the electronic structure of a material responds to

perturbations on femtosecond time scales. Here we report a unique ultrafast time-resolved ARPES study of a high- T_c cuprate superconductor. Compared to previous time-resolved studies,¹⁶⁻¹⁸ the primary advantage of this work is an unprecedented momentum (angular) resolution ($\Delta k \sim 0.003$ vs. 0.05 \AA^{-1}), on par with that of state-of-the-art ARPES. This has allowed the time-resolved measurement of significantly sharper QP spectral peaks with strikingly larger peak-to-background ratios than previously reported.¹⁶ Additionally, a lower pump fluence is used ($\lesssim 40 \mu\text{J}/\text{cm}^2$ vs. $\sim 100 \mu\text{J}/\text{cm}^2$), which reduces pump-induced sample temperature increase and related thermal smearing of spectral features. This allows us to uncover a surprising meltdown of nodal QP spectral weight following pump laser excitation. This meltdown is only observed in the superconducting state and for QPs with binding energy less than the kink energy,¹⁹ revealing a link between nodal QPs and superconductivity.

NODAL QUASIPARTICLE RESPONSE TO PHOTOEXCITATION

The experiment proceeds as follows. A pump laser pulse ($h\nu = 1.5 \text{ eV}$) excites electrons from occupied to unoccupied states within 1.5 eV of the Fermi energy (E_F). As shown by previous ultrafast optical studies, the photoexcited carriers relax to states near E_F within 100 fs, generating a large non-equilibrium population of QPs and a depletion of the superconducting condensate.²⁰⁻²⁹ The subsequent recombination of these non-equilibrium QPs is detected via photoemission with a probe laser pulse ($h\nu = 5.9 \text{ eV}$) as a function of a variable time delay between the pump and probe. The laser pulse widths provide a time resolution $\approx 270 \text{ fs}$.

Figure 1 compares the equilibrium electronic structure (before the arrival of the pump pulse) with the transient excited electronic structure at $t = 0.3 \text{ ps}$ after excitation, above and below the superconducting transition. For the low (high) temperature data, the bulk sample temperature was measured to be $T = 20 \text{ K}$ (120 K) with a diode thermally connected to the crystal, and was found not to be measurably affected by the photoexcitation. Low temperature ARPES intensity maps (energy vs. momentum) of the equilibrium and transient states are shown in panels (a) and (b), respectively, with identical color

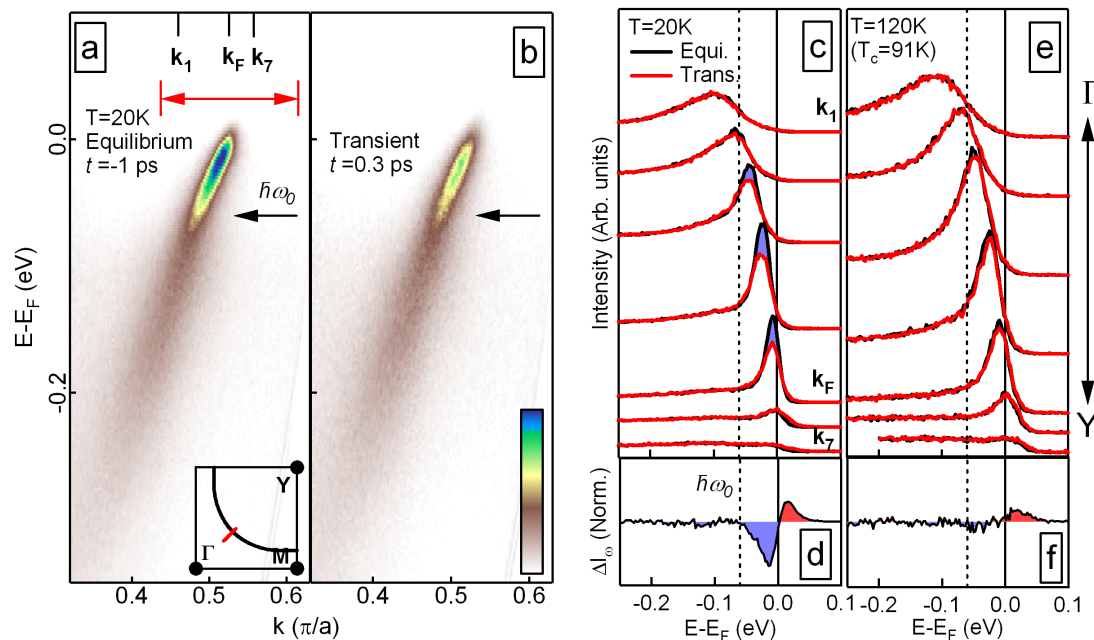


FIG. 1. Nodal QP spectral weight suppression after an infrared pump pulse. (a) Energy-momentum map of equilibrium ARPES intensity before the pump pulse (negative delay time). The momentum location of the cut is shown on the Fermi surface inset. The well known dispersion kink is marked by the arrow. (b) Corresponding map of the transient ARPES intensity 0.3 ps after the pump pulse. The same color scale is used for both panels. (c) Energy distribution curves (EDCs) from k_1 to k_7 for the equilibrium (a, in black) and transient state (b, in red). Each EDC pair is separated by the same momentum value and vertically displaced by different amounts for clarity. Spectral weight loss (gain) is highlighted by the blue (red) areas. (d) ΔI_ω , the difference between the transient and equilibrium EDCs, integrated through a momentum range centered around k_F and shown by the red double arrow in (a). (e-f) Same comparison as in panel (c-d) but with the equilibrium sample temperature at 120 K ($T_c = 91$ K). (f) Plot is shown on the same scale as (d).

scales. In both maps, one can identify a characteristic binding energy ($|E - E_F| \hbar\omega_0 \sim 60$ meV (marked by arrows) that separates a low binding energy region between E_F and $\hbar\omega_0$ characterized by a sharply defined dispersive peak, from a high binding energy region characterized by a poorly defined dispersive peak. The crossover energy $\hbar\omega_0$ also marks the energy position of a kink in the nodal QP dispersion, which is a universal feature of the cuprates.¹⁹ An obvious pump-induced suppression of spectral intensity occurs which appears to be strictly confined to the low binding energy region (binding energy $< \hbar\omega_0$).

The data are compared more directly in panel (c), which shows raw energy distribution curves (EDCs - photoemission intensity as a function of energy at constant momentum) for the equilibrium (black) and transient (red) states, corresponding to the maps in panels (a) and (b), respectively. The EDCs are normalized only by the total acquisition time and not by any additional high binding energy normalization scheme, and so a direct intensity comparison can accurately be made. As in (a) and (b), the characteristic energy $\hbar\omega_0$ (marked by the vertical dotted line) separates sharp peaks from broad ones. The sharp spectral peaks are signatures of coherent QPs.

The advantage of the high momentum resolution of the current work is clearly seen by the sharpness and intensity of the QP peaks. Again, there is a clear suppression of spectral weight in the transient state, confined to the QPs at binding energies less than $\hbar\omega_0$.

Such suppression cannot be explained by thermal smearing of the Fermi edge due to the transient heating of the electronic temperature caused by the absorbed pump energy. We find that the transient electrons around E_F quickly thermalize and follow a Fermi-Dirac distribution within 100 fs of the ultrafast pump pulse, in close agreement with Ref. 16. Therefore the transient electronic temperature at each delay time can be obtained by direct measurement of the Fermi edge width of the corresponding transient ARPES signal (see Supplementary Information for details). The electronic temperature of the transient data of Fig. 1 is thus found to be < 100 K, and does not account for the observed spectral changes. This is clear from Fig. 1(c) by the significant loss of spectral weight at binding energies larger than $4k_B T = 34$ meV, which therefore cannot be attributed to Fermi edge thermal smearing.

Panel (d) shows the difference of the transient and equilibrium EDCs (ΔI_ω), integrated through a wide mo-

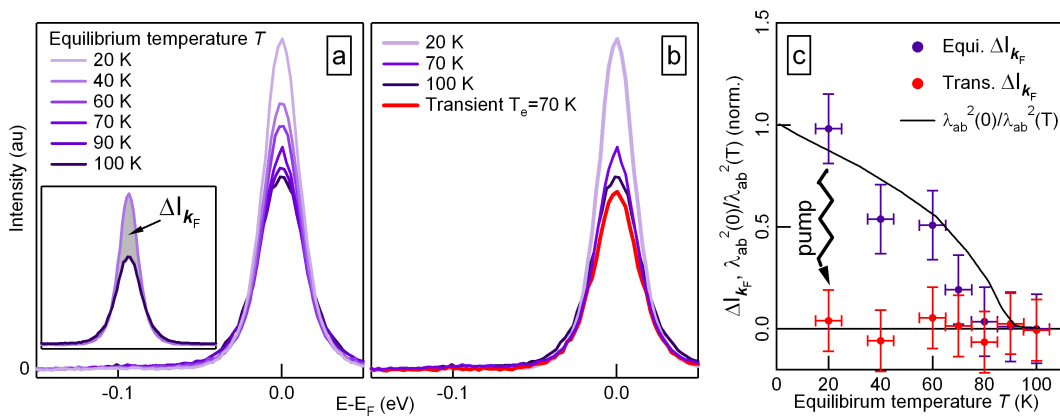


FIG. 2. Comparison between equilibrium temperature driven and optical pump driven spectral weight suppression. (a) Symmetrized equilibrium EDCs at \mathbf{k}_F along the nodal direction at several equilibrium temperatures. The inset defines $\Delta I_{\mathbf{k}_F}$ as the area difference between two EDCs. (b) Selected equilibrium EDCs from (a) compared with a transient EDC with an equilibrium temperature of 20 K and a transient electronic temperature of 70 K. (c) Equilibrium and transient $\Delta I_{\mathbf{k}_F}$ as a function of equilibrium temperature. The superfluid density estimated from the penetration depth, λ_{ab} , measured by microwave spectroscopy [adapted from Ref. 31] is shown for comparison. The equilibrium and transient values of $\Delta I_{\mathbf{k}_F}$ are normalized by the equilibrium value of $\Delta I_{\mathbf{k}_F}$ at 20 K. The vertical error bars are based on the uncertainty on the determination of \mathbf{k}_F , and the horizontal error bars are a generous estimation of error in the equilibrium temperature measured by silicon diode and a small temperature gradient between the diode and sample.

mentum range that captures the extent of observed spectral changes. The negative blue (positive red) area under the curve illustrates the total nodal spectral weight lost (gained) after pumping as a function of binding energy. Again, this clearly shows that photoinduced spectral change is confined to binding energies less than the kink energy, $\hbar\omega_0$. Although it appears that the spectral loss (blue area) is larger than the spectral gain (red area), we note that such a comparison involves regions of vastly different signal intensities as the count rate below E_F is far larger than that above. Even small non-linearity effects common to the typical photoelectron detectors used³⁰ may impact the relative magnitudes of the measured ΔI_{ω} above and below E_F .

In panels (e) and (f), we present a similar comparison of EDCs associated with equilibrium and transient states, but this time with an equilibrium temperature of 120 K, above the superconducting transition $T_c = 91$ K. Like the low temperature data, $\hbar\omega_0$ separates sharp QP peaks from broad spectral features, and the QP peak sharpens as momentum $\mathbf{k} \rightarrow \mathbf{k}_F$ ($E \rightarrow E_F$). The transient state also has an elevated electronic temperature, here determined to be ~ 145 K (see Supplementary Information). In sharp contrast to panels (c,d), we do not observe a significant change in the transient state's QP spectral features in panels (e,f). This shows that the surprising pump-induced loss of nodal QP spectral weight is dramatically sensitive to the superconducting state.

NODAL QUASIPARTICLE TEMPERATURE DEPENDENCE

In Figure 2 we investigate the role of transient heating by the pump pulses in the nodal QP spectral weight suppression. This was done by performing a standard equilibrium temperature dependence. Panel (a) shows the resulting EDCs, symmetrized about E_F , at \mathbf{k}_F for several temperatures from 20 K to above T_c . The symmetrization removes thermal effects that enter through the Fermi-Dirac distribution by effectively canceling out the Fermi-Dirac function.³² Unlike previous synchrotron data,^{13–15} our laser data show a substantial dependence of the nodal QP spectral weight on temperature. This remarkable new observation, which is likely due to the enhanced bulk sensitivity achieved with relatively low photon energy by laser-ARPES,³³ on its own challenges the notion of complete robustness of nodal QPs.

In panel (b), we directly compare the temperature dependence of the equilibrium QP spectral weight with pump-induced spectral weight suppression. Here, the electronic temperature of the pumped transient state is 70 ± 5 K. As described above, the transient electronic temperature is obtained by the direct measurement of the Fermi edge width of the transient ARPES signal (see Supplementary Information for details). The lower transient electronic temperature relative to that in Fig. 1 was achieved by reducing the fluence of the pump pulse from ~ 40 to ~ 25 $\mu\text{J}/\text{cm}^2$. Although the electronic temperature of the transient EDC is only ~ 70 K, it exhibits a similar or greater loss of spectral weight than the 100 K equilibrium EDC. This suggests that optical pumping in-

duces a measurable effect beyond what is consistent with merely increasing the sample temperature. This suggests that the transient nodal QP spectral weight does not simply follow the transient electronic temperature, a concept which is consistent with the fact that the transient state is not at equilibrium. However, it should be noted that the inherent difficulties of precise comparisons of equilibrium temperature dependent data (e.g. maintaining the same sample spot and momentum-space position) place significant error bars on such direct comparisons (see Fig. 3c).

In panel (c) we compare the equilibrium bulk temperature dependence of the QP spectral weight suppression in the equilibrium and transient states. Here we define the equilibrium (transient) $\Delta I_{\mathbf{k}_F}$ as the difference between the areas under the equilibrium (transient) EDC at T and the equilibrium (transient) normal state EDC ($T = 100$ K). (See illustration in the inset of Fig. 2(a).) We make the following two observations: (1) the equilibrium value of $\Delta I_{\mathbf{k}_F}$ (purple markers) has a temperature dependence which is remarkably similar to the antinodal QP spectral weight^{2,3} and to the superfluid density, shown for comparison in the same figure (solid black line); and (2) the transient state $\Delta I_{\mathbf{k}_F}$ (red markers) is temperature independent. Point (1) suggests that the equilibrium value of $\Delta I_{\mathbf{k}_F}$ is proportional to the superfluid density. This finding is quite surprising as it contradicts the conventional view that the nodal QPs are uninvolved with and insensitive to superconductivity, and argues that the dichotomy between nodal and antinodal QPs is not as extensive as often thought. However, despite the similarity between the temperature dependence of the nodal and antinodal QP spectral weight, there remain two important distinctions. First, the antinodal QP peak is almost entirely suppressed above T_c while a finite component of the nodal QP peak is robust and persists above T_c . Second, the antinodal QP peak, despite its strong temperature dependence, is believed to satisfy a sum rule³⁴ (the total spectral weight at a given momentum is conserved). In contrast, our data show that the nodal QP peak spectral weight is not conserved within our experimentally accessible energy window, either with increasing equilibrium temperature or with photoexcitation. It is possible that the missing spectral weight is redistributed to higher energies and/or different momenta³⁵⁻³⁷, for instance to the antinodal region.

These findings suggest that the transient state superfluid density is nearly zero regardless of the equilibrium temperature. Indeed it is well established by ultrafast THz experiments that an optical pump pulse can induce a suppression of superfluid density in the transient state,^{24,38} and the current saturation effect is consistent with other optical pump-probe experiments that have found the depletion of the superconducting condensate is nearly complete at pump fluences below what is used here.^{25,39} In addition, the fact that the transient state nodal spectral weight is very similar to the equilibrium nodal spectral weight in the normal state also supports the conclusion that the transient state superfluid density

has been suppressed to zero by the optical pump while the electronic temperature is below T_c . Again, we stress that the transient state is not in equilibrium, and that these observations may reflect the possibility that the electronic temperature cools at a faster rate than the superconducting condensate reforms. Such an effect may be expected in this non-equilibrium state since the rate of condensate formation is additionally constrained by energy and momentum conservation of the quasiparticle interactions underlying the charge pairing.

DYNAMICS OF NODAL QUASIPARTICLE RESPONSE

In Figure 3 we report the recovery of the nodal QP spectral weight as a function of delay time, determined from the angle-integrated photoemission intensity for an equilibrium temperature of 20 K. To focus on spectral change, we show the spectral intensity with the equilibrium data ($t = -1$ ps) subtracted. Similar to Figs. 1(d,f), panel (a) shows the angle integrated spectral intensity change between transient and equilibrium EDCs, ΔI_ω , at various delay times, with the curve at $t = -1$ ps being exactly flat by definition. Panel (b) shows a false-color map of the spectral intensity change, built up by ΔI_ω curves at many delay times. Two main features appear in both panels: a pump-induced increase in spectral intensity above E_F (red feature) that can be partially understood as the thermally excited population of the states above E_F , and a spectral weight suppression confined between E_F and $\hbar\omega_0$ (blue feature).

The dynamics of these spectral changes, ΔI_e and ΔI_h , are shown in panel (c) integrated through the energy ranges marked by the red and blue arrows, respectively, in (b). The total change in spectral weight, ΔI , is integrated through the energy range marked by the black arrow. The dashed and solid gray lines are single exponential least-square fits to ΔI_e and ΔI_h with time constants of 2.4 and 2.8 ps, respectively. These values agree well with those observed at similar pump fluences in optical reflectivity measurements of underdoped $\text{Bi}_2\text{Sr}_2\text{CaCu}_2\text{O}_{8+\delta}$.²⁹ The two dynamics are shown renormalized and on a log scale in the inset to provide a more direct comparison, and a difference in dynamics is observed. Indeed, ΔI_e appears to have a kink, indicating an additional, fast component which is not apparent in ΔI_h , although improved statistics are required to more accurately determine this aspect in future works. In a simple approach, one may expect that the dynamics are governed by multiple components, one of which is purely controlled by the electronic temperature through the smearing of the Fermi edge and acts symmetrically above and below E_F , while other components may reflect dynamics which do not trivially follow the electronic temperature.

In panel (d) we show the time dependence of the transient electronic temperature, T_e , determined by fitting

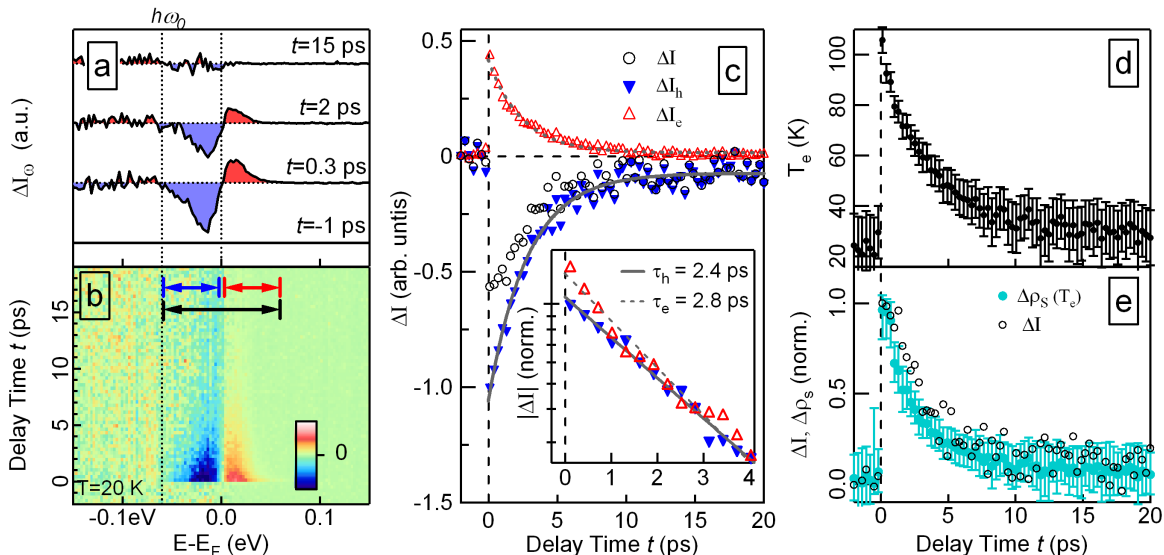


FIG. 3. Time dependence of the pump-induced spectral changes for an equilibrium temperature of $T = 20$ K. (a) ΔI_ω , the difference of transient and equilibrium EDCs, integrated through the momentum range shown by the red double arrow in Fig. 1, equivalent to Fig. 1(d), at various delay times. The curves are shifted vertically for clarity. (b) Color map of ΔI_ω as a function of delay times. The curves in (a) are horizontal intensity profiles from (b). (c) Angle and energy integrated spectral weight changes (ΔI). Open red triangles (filled blue triangles) correspond to the change in spectral intensity above (below) E_F , termed electrons (holes), and correspond to vertical intensity profiles of ΔI_ω in (b), integrating along the energy range spanned by the red (blue) double arrow. The solid and dashed gray lines are exponential fits. The open black circles correspond to the sum of the red and blue triangles, or integrating ΔI_ω along the energy range spanned by the black double arrow. The inset compares the ΔI_e and ΔI_h dynamics in a smaller time range, with ΔI_e inverted and normalized. (d) Electronic temperature T_e determined from the width of the Fermi-Dirac distribution as a function of delay time. The error bars are from the fit standard deviation and the uncertainty in the experimental resolution and the space charging contribution⁴⁰. (e) ΔI (black circles from (c)) compared with the estimated minimal change of superfluid density ($\Delta\rho_s(T_e)$) (see text) as a function of delay time (light blue markers).

the Fermi edge of the angle-integrated data at the node with a Fermi-Dirac distribution function. The time dependence shows that the equilibrium temperature of 20 K is recovered before the following pump pulse, $\sim 1\mu\text{s}$ later. This guarantees that there is minimal residual heating from pulse to pulse in all our experiments. When these transient electronic temperature data are combined with microwave spectroscopy data of the superfluid density³¹ shown in Fig. 2(c), a minimum value for the change in the superfluid density ($\Delta\rho_s(T_e)$), based solely on the electronic temperature, is obtained and shown in light blue in Fig. 3 (e). This is directly compared with the normalized absolute value of the net ΔI from panel (c). The similarity between the net ΔI and $\Delta\rho_s(T_e)$ in this panel is consistent with our proposal that the lost nodal spectral weight is proportional to the superfluid density. More precisely, the fact that ΔI does not decay on a faster time scale than $\Delta\rho_s(T_e)$ is also consistent with this proposal. That the data possibly show that the dynamics of ΔI lag behind $\Delta\rho_s(T_e)$ may also be consistent with the notion that the time scale for Cooper pair formation in $\text{Bi}_2\text{Sr}_2\text{CaCu}_2\text{O}_{8+\delta}$ ²³ occurs at slower time scales than the present decay of the electronic temperature, thus limiting the decay of ΔI to be slower than that of $\Delta\rho_s(T_e)$. How-

ever, better statistics in future works are necessary for a more rigorous comparison to establish the exact dynamic of ΔI .

In summary, we propose that the observed temperature- and/or pump- driven suppression of QP spectral weight is due to an increase in superconducting Cooper pair phase fluctuations^{41–43} corresponding to a loss in superfluid density. Further work with this approach is motivated to expand the study to other regions of momentum space as one may expect the behavior to be different towards the antinode.

METHODS

Pump and probe photon beams were generated from a cavity-dumped, mode-locked Ti:Sapphire oscillator (Coherent Mira) providing ~ 150 fs pulses of 840 nm at $\lesssim 1$ MHz repetition rate. A fraction of the beam was variably delayed and focused onto the sample as the pump with a spot size of $100\mu\text{m}$ diameter and fluences up to $40\mu\text{J}/\text{cm}^2$. The remaining beam was frequency quadrupled to form the probe beam with $h\nu = 5.9$ eV and a measured bandwidth of 15 meV and focused onto the same

sample spot with a size of $\sim 40 \times 60 \mu\text{m}$. The combined beams were cross-correlated in time with a FWHM of 0.27 ps.

ARPES measurements were taken with a 150 mm hemispherical analyzer with 2D imaging detector (SPECS Phoibos 150). The total experimental energy resolution, including probe beam bandwidth, was measured to be 21 meV. The angular resolution of $< 0.3^\circ$ along the nodal direction corresponds to a momentum resolution of $< 0.003 \text{ \AA}^{-1}$ at the given photoelectron kinetic energies and emission angles. Probe and pump photons were s-polarized, with the polarization vector perpendicular to the direction of the nodal momentum space cut measured.

Samples were mounted on a 6-axis manipulator, cleaved at 4×10^{-11} torr, and directly oriented by taking ARPES Fermi surface maps. The data for Figs. 1(a-d) and 3 are from samples cleaved and maintained at 20 K, the data for Figs. 1(e-f) are from samples cleaved and maintained at 120 K, and the data for Fig. 2 are from a sample cleaved at 100 K, with the T dependence taken at sequentially lower temperatures.

CORRESPONDENCE

Correspondence and requests for materials should be addressed to A.L.

ACKNOWLEDGMENTS

We thank Z. Hussain for support in the initial stage of the project and J. Orenstein and W. Zhang for useful discussions. This work was supported by the Director, Office of Science, Office of Basic Energy Sciences, Materials Sciences and Engineering Division, of the U.S. Department of Energy under Contract No. DE-AC02-05CH11231.

AUTHOR CONTRIBUTIONS

J.G. and C.J. designed and built the laser-ARPES system. R.A.K. contributed to the design concept of the laser-ARPES system. J.G. carried out the experiment. J.G., C.J., and C.S. are responsible for data analysis. H.E. prepared the samples. A.L. is responsible for the experimental concept, planning, and infrastructure. All authors contributed to the interpretation and manuscript.

ADDITIONAL INFORMATION

The authors declare that they have no competing financial interests. Supplementary Information accompanies this paper.

* These authors contributed equally to this work.

† ALanzara@lbl.gov

¹ Damascelli, A., Hussain, Z. & Shen, Z.-X. Angle-resolved photoemission studies of the cuprate superconductors. *Rev. of Mod. Phys.* **75**, 473–541 (2003).

² Feng, D. L. *et al.* Signature of superfluid density in the single-particle excitation spectrum of $\text{Bi}_2\text{Sr}_2\text{CaCu}_2\text{O}_{8+\delta}$. *Science* **289**, 277–281 (2000).

³ Ding, H. *et al.* Coherent quasiparticle weight and its connection to high- T_c superconductivity from angle-resolved photoemission. *Phys. Rev. Lett.* **87**, 227001 (2001).

⁴ Garg, A., Randeria, M. & Trivedi, N. Strong correlations make high-temperature superconductors robust against disorder. *Nat Phys* **4**, 762–765 (2008).

⁵ Pan, S. H. *et al.* Microscopic electronic inhomogeneity in the high- T_c superconductor $\text{Bi}_2\text{Sr}_2\text{CaCu}_2\text{O}_{8+x}$. *Nature* **413**, 282–285 (2001).

⁶ McElroy, K. *et al.* Coincidence of Checkerboard Charge Order and Antinodal State Decoherence in Strongly Underdoped Superconducting $\text{Bi}_2\text{Sr}_2\text{CaCu}_2\text{O}_{8+\delta}$. *Phys. Rev. Lett.* **94**, 197005 (2005).

⁷ Ando, Y., Lavrov, A. N., Komiya, S., Segawa, K. & Sun, X. F. Mobility of the doped holes and the antiferromagnetic correlations in underdoped high- T_c cuprates. *Phys. Rev. Lett.* **87**, 017001 (2001).

⁸ Zhou, X. J. *et al.* High-temperature superconductors: Universal nodal Fermi velocity. *Nature* **423**, 398 (2003).

⁹ Gweon, G.-H. *et al.* An unusual isotope effect in a high-transition-temperature superconductor. *Nature* **430**, 187–

190 (2004).

¹⁰ Shen, K. M. *et al.* Nodal Quasiparticles and Antinodal Charge Ordering in $\text{Ca}_{2-x}\text{Na}_x\text{CuO}_2\text{Cl}_2$. *Science* **307**, 901–904 (2005).

¹¹ Vershinin, M. *et al.* Local ordering in the pseudogap state of the high- T_c superconductor $\text{Bi}_2\text{Sr}_2\text{CaCu}_2\text{O}_{8+\delta}$. *Science* **303**, 1995–1998 (2004).

¹² Valla, T. *et al.* Evidence for quantum critical behavior in the optimally doped cuprate $\text{Bi}_2\text{Sr}_2\text{CaCu}_2\text{O}_{8+\delta}$. *Science* **285**, 2110–2113 (1999).

¹³ Yusof, Z. M. *et al.* Quasiparticle liquid in the highly overdoped $\text{Bi}_2\text{Sr}_2\text{CaCu}_2\text{O}_{8+\delta}$. *Phys. Rev. Lett.* **88**, 167006 (2002).

¹⁴ Wei, J. *et al.* Superconducting coherence peak in the electronic excitations of a single-layer $\text{Bi}_2\text{Sr}_{1.6}\text{La}_{0.4}\text{CuO}_{6+\delta}$ cuprate superconductor. *Phys. Rev. Lett.* **101**, 097005 (2008).

¹⁵ Kondo, T., Khasanov, R., Takeuchi, T., Schmalian, J. & Kaminski, A. Competition between the pseudogap and superconductivity in the high- T_c copper oxides. *Nature* **457**, 296–300 (2009).

¹⁶ Perfetti, L. *et al.* Ultrafast electron relaxation in superconducting $\text{Bi}_2\text{Sr}_2\text{CaCu}_2\text{O}_{8+\delta}$ by time-resolved photoelectron spectroscopy. *Phys. Rev. Lett.* **99**, 197001 (2007).

¹⁷ Schmitt, F. *et al.* Transient electronic structure and melting of a charge density wave in TbTe_3 . *Science* **321**, 1649–1652 (2008).

¹⁸ Rettig, L. *et al.* Electron-phonon coupling and momentum dependent electron dynamics in EuFe_2As_2 using time-

- and angle-resolved photoemission spectroscopy. Preprint at <http://arxiv.org/abs/1008.1561v2> (2010).
- ¹⁹ Lanzara, A. *et al.* Evidence for ubiquitous strong electron-phonon coupling in high-temperature superconductors. *Nature* **412**, 510–514 (2001).
 - ²⁰ Han, S. G., Vardeny, Z. V., Wong, K. S., Symko, O. G. & Koren, G. Femtosecond optical detection of quasiparticle dynamics in high- T_c $\text{YBa}_2\text{Cu}_3\text{O}_{7-\delta}$ superconducting thin films. *Phys. Rev. Lett.* **65**, 2708–2711 (1990).
 - ²¹ Stevens, C. J. *et al.* Evidence for two-component high-temperature superconductivity in the femtosecond optical response of $\text{YBa}_2\text{Cu}_3\text{O}_{7-\delta}$. *Phys. Rev. Lett.* **78**, 2212–2215 (1997).
 - ²² Demsar, J., Podobnik, B., Kabanov, V. V., Wolf, T. & Mihailovic, D. Superconducting gap Δ_c , the pseudogap Δ_p , and pair fluctuations above T_c in overdoped $\text{Y}_{1-x}\text{Ca}_x\text{Ba}_2\text{Cu}_3\text{O}_{7-\delta}$ from femtosecond time-domain spectroscopy. *Phys. Rev. Lett.* **82**, 4918–4921 (1999).
 - ²³ Kaindl, R. A. *et al.* Ultrafast mid-infrared response of $\text{YBa}_2\text{Cu}_3\text{O}_{7-\delta}$. *Science* **287**, 470–473 (2000).
 - ²⁴ Averitt, R. D. *et al.* Nonequilibrium superconductivity and quasiparticle dynamics in $\text{YBa}_2\text{Cu}_3\text{O}_{7-\delta}$. *Phys. Rev. B* **63**, 140502(R) (2001).
 - ²⁵ Segre, G. P. *et al.* Photoinduced changes of reflectivity in single crystals of $\text{YBa}_2\text{Cu}_3\text{O}_{6.5}$ (ortho ii). *Phys. Rev. Lett.* **88**, 137001 (2002).
 - ²⁶ Gedik, N., Orenstein, J., Liang, R., Bonn, D. A. & Hardy, W. N. Diffusion of nonequilibrium quasi-particles in a cuprate superconductor. *Science* **300**, 1410–1412 (2003).
 - ²⁷ Gedik, N. *et al.* Single-quasiparticle stability and quasiparticle-pair decay in $\text{YBa}_2\text{Cu}_3\text{O}_{6.5}$. *Phys. Rev. B* **70**, 014504 (2004).
 - ²⁸ Kusar, P. *et al.* Controlled vaporization of the superconducting condensate in cuprate superconductors by femtosecond photoexcitation. *Phys. Rev. Lett.* **101**, 227001 (2008).
 - ²⁹ Liu, Y. H. *et al.* Direct observation of the coexistence of the pseudogap and superconducting quasiparticles in $\text{Bi}_2\text{Sr}_2\text{CaCu}_2\text{O}_{8+y}$ by time-resolved optical spectroscopy. *Phys. Rev. Lett.* **101**, 137003 (2008).
 - ³⁰ Mannella, N. *et al.* Correction of non-linearity effects in detectors for electron spectroscopy. *J. Electron Spectrosc. Relat. Phenom.* **141**, 45–59 (2004).
 - ³¹ Jacobs, T., Sridhar, S., Li, Q., Gu, G. D. & Koshizuka, N. In-plane and c-axis microwave penetration depth of $\text{Bi}_2\text{Sr}_2\text{CaCu}_2\text{O}_{8+\delta}$ crystals. *Phys. Rev. Lett.* **75**, 4516–4519 (1995).
 - ³² Norman, M. R. *et al.* Destruction of the fermi surface in underdoped high- T_c superconductors. *Nature* **392**, 157–160 (1998).
 - ³³ Casey, P. A., Koralek, J. D., Plumb, N. C., Dessau, D. S. & Anderson, P. W. Accurate theoretical fits to laser-excited photoemission spectra in the normal phase of high-temperature superconductors. *Nat. Phys.* **4**, 210–212 (2008).
 - ³⁴ Randeria, M. *et al.* Momentum distribution sum rule for angle-resolved photoemission. *Phys. Rev. Lett.* **74**, 4951–4954 (1995).
 - ³⁵ Basov, D. N. *et al.* Sum rules and interlayer conductivity of high- T_c cuprates. *Science* **283**, 49–52 (1999).
 - ³⁶ Molegraaf, H. J. A., Presura, C., van der Marel, D., Kes, P. H. & Li, M. Superconductivity-induced transfer of in-plane spectral weight in $\text{Bi}_2\text{Sr}_2\text{CaCu}_2\text{O}_{8+\delta}$. *Science* **295**, 2239–2241 (2002).
 - ³⁷ Phillips, P., Galanakis, D. & Stanescu, T. D. Absence of asymptotic freedom in doped Mott insulators: Breakdown of strong coupling expansions. *Phys. Rev. Lett.* **93**, 267004 (2004).
 - ³⁸ Kaindl, R. A., Carnahan, M. A., Chemla, D. S., Oh, S. & Eckstein, J. N. Dynamics of cooper pair formation in $\text{Bi}_2\text{Sr}_2\text{CaCu}_2\text{O}_{8+\delta}$. *Phys. Rev. B* **72**, 060510(R) (2005).
 - ³⁹ Carnahan, M. A. *et al.* Nonequilibrium thz conductivity of $\text{Bi}_2\text{Sr}_2\text{CaCu}_2\text{O}_{8+\delta}$. *Phys. C* **408–410**, 729–730 (2004).
 - ⁴⁰ Graf, J. *et al.* Vacuum space charge effect in laser-based solid-state photoemission spectroscopy. *J. Appl. Phys.* **107**, 014912 (2010).
 - ⁴¹ Emery, V. J. & Kivelson, S. A. Importance of phase fluctuations in superconductors with small superfluid density. *Nature* **374**, 434–437 (1995).
 - ⁴² Corson, J., Mallozzi, R., Orenstein, J., Eckstein, J. N. & Bozovic, I. Vanishing of phase coherence in underdoped $\text{Bi}_2\text{Sr}_2\text{CaCu}_2\text{O}_{8+\delta}$. *Nature* **398**, 221–223 (1999).
 - ⁴³ Khodas, M. & Tsvetlik, A. M. Influence of thermal phase fluctuations on the spectral function for a two-dimensional d-wave superconductor. *Phys. Rev. B* **81**, 094514 (2010).